Applied Catalysis B: Environmental 144 (2014) 622–630

Contents lists available at ScienceDirect

Applied Catalysis B: Environmental

journal homepage: www.elsevier.com/locate/apcatb

# Using electrochemical methods to study the promotion mechanism of the photoelectric conversion performance of Ag-modified mesoporous g-$C_3N_4$ heterojunction material

Yuyu Bu [a], Zhuoyuan Chen [a,*], Weibing Li [b]

[a] Key Laboratory of Marine Environmental Corrosion and Bio-fouling, Institute of Oceanology, Chinese Academy of Sciences, 7 Nanhai Road, Qingdao 266071, PR China
[b] School of Environment and Safety Engineering, Qingdao University of Science and Technology, 53 Zhengzhou Road, Qingdao 266042, PR China

ARTICLE INFO

*Article history:*
Received 30 May 2013
Received in revised form 24 July 2013
Accepted 28 July 2013
Available online 7 August 2013

*Keywords:*
mg-$C_3N_4$
Ag
Heterojunction
Electrochemical test methods
Visible light

ABSTRACT

Silver (Ag) nanoparticles are successfully modified onto mesoporous graphitic carbon nitride (mg-$C_3N_4$) by photo-assisted reduction. Modifying mg-$C_3N_4$ with Ag significantly increases the photoelectric conversion performance. The promotion mechanism is studied through electrochemical methods for the first time. Modifying mg-$C_3N_4$ with Ag also increases the conductivity and lowers the energy barrier of the interface reactions. A heterojunction electric field, forms on the interface between the modified Ag and mg-$C_3N_4$, enhances the separation efficiency of photogenerated electron–hole pairs. The enhanced separation efficiency thus prolongs the lifetime of the photogenerated electrons and significantly improves the photoelectric conversion performance of mg-$C_3N_4$. Furthermore, Modifying mg-$C_3N_4$ with Ag significantly improves the adsorption capacity and photocatalytic degradation efficiency. Smaller Ag nanoparticles are much more effective than larger ones in improving photoelectric conversion performance.



## 1. Introduction

With the depletion of energy and the aggravation of global environmental pollution, the development and utilization of new energy resources and environmental improvements have become the major concerns of the present era. The photocatalytic degradation of organic pollutants, developed over the past 40 years, is undoubtedly an ideal environmental improvement and solar energy-based technology [1,2]. $TiO_2$ and ZnO with various nanotopographies have been widely studied in the photocatalytic degradation of organic pollutants [3–6], photoelectrochemical hydrogen production from water splitting [7–11], and production of dye-sensitized solar cells [12–14]. However, these semiconductor materials are seriously mismatched with the solar spectrum because of their UV light-response characteristics. Thus, many studies have involved the doping of $TiO_2$ and ZnO with metallic and/or non-metallic elements [15–17] and combined them with other semiconductor materials with narrow bandgaps [18,19] to achieve their visible-light response. Moreover, researchers have also explored novel stable and non-toxic visible light-responsive semiconductor materials. For example, $BiVO_4$ [20,21], $Bi_2WO_4$ [22,23], and $ZnFe_2O_4$ [24,25] have been reported to possess visible light photocatalytic properties.

Wang et al. [26] reported that graphite-like carbon nitride (g-$C_3N_4$) possessed photocatalytic properties for hydrogen and oxygen production by water splitting under visible light. Thereafter, several studies have doped g-$C_3N_4$ with other elements and prepared it with special nano-topographies to further enhance its photoelectric conversion property. Wang et al. [27] introduced impurity levels into g-$C_3N_4$ by doping it with Fe and found that Fe-doped g-$C_3N_4$ possessed a wider optical absorption range and better photocatalytic degradation performance than undoped g-$C_3N_4$. Zhang et al. [28] doping g-$C_3N_4$ with graphene significantly increases its photoelectric conversion ability, and the doped material has a potential application value in optoelectronic areas. Zhang et al. [29] found that the light absorption range of P-doped g-$C_3N_4$ extended to the near-infrared region, and its electrical conductivity significantly improved. Goettmann et al. [30] and Wang et al. [31] prepared mesoporous g-$C_3N_4$ (mg-$C_3N_4$) and also found that the capacity for photoelectrochemical hydrogen production from the water splitting of mg-$C_3N_4$ significantly improved.

The photocatalytic properties of a metal–semiconductor heterojunction prepared by modifying metals, such as silver (Ag), gold (Au), platinum (Pt), and nickel (Ni) onto a semiconductor can be significantly improved [32–36]. Ge et al. [37] prepared Ag-modified g-$C_3N_4$ heterojunction composite and found that the modification

* Corresponding author. Tel.: +86 53282898731; fax: +86 53282880498.
*E-mail address:* zychen@qdio.ac.cn (Z. Chen).

0926-3373/$ – see front matter © 2013 Elsevier B.V. All rights reserved.
http://dx.doi.org/10.1016/j.apcatb.2013.07.066

of Ag on the g-$C_3N_4$ surface significantly enhanced the visible-light photocatalytic capacity of g-$C_3N_4$. The increased capacity was attributed to the simultaneous optimization of electron transfer and chemical reactivity by Ag modification. However, Ge et al. [37] did not discuss the synergistic effect and interactions between Ag and g-$C_3N_4$, which can provide theoretical basis for furthering the optimization of the photoelectric conversion efficiency of g-$C_3N_4$. In the present paper, the authors modified different amounts of Ag nanoparticles onto the mg-$C_3N_4$ surface through photo-assisted reduction and studied the degradation performance for Rhodamine B (RhB) of the prepared series photocatalysts under visible light. Photoelectrodes were prepared by evenly depositing mg-$C_3N_4$ and Ag-modified mg-$C_3N_4$ (Ag/mg-$C_3N_4$) powder onto the surface of fluorine-doped tin-oxide (FTO) conductive glasses. The mechanism of the improvement of the photoelectric conversion efficiency of mg-$C_3N_4$ by Ag modification was studied for the first time through electrochemical methods.

## 2. Experimental

### 2.1. Preparation of mg-$C_3N_4$ and Ag/mg-$C_3N_4$ powder

The preparation of mg-$C_3N_4$ and Ag/mg-$C_3N_4$ powder was based on the method used by Goettmann et al. [30]. First, 1.2 g silicon dioxide ($SiO_2$) nanopowder with a diameter of approximately 15 nm was dispersed in 20 mL deionized water, and the resulting mixture was ultrasonically vibrated for 30 min. This dispersion liquid was added slowly to a dicyanodiamine solution prepared by dissolving 3 g dicyanodiamine in 20 mL deionized water. The liquid mixture was stirred in a 70 °C water bath until the water in the liquid mixture was completely evaporated. The dried powder was ground in an agate mortar, transferred to a crucible with a lid, and heated at 520 °C for 4 h at a heating rate of 20 °C $min^{-1}$. The light-yellow powder generated after sintering was added to 100 mL of 4 mol $L^{-1}$ $NH_4F$ solution and etched for 24 h. The powder was then filtered and repeatedly washed with deionized water. A yellow powder was obtained after drying at 80 °C for 4 h under vacuum conditions. Ag nanoparticles were modified onto the surface of the prepared mg-$C_3N_4$ by photo-assisted reduction. Silver nitrate ammonia (SNA) solution was made by dissolving a certain amount of $AgNO_3$ based on the Ag modifying amount into 2 mL $NH_4OH$ (25 wt% $NH_3$). One gram (1 g) of the prepared mg-$C_3N_4$ was ultrasonically dispersed in 40 mL deionized water for 20 min. Subsequently, this dispersion liquid was swiftly added to the prepared SNA solution and stirred well. The solution was transferred into a beaker with a controlled temperature of 25 °C with a water cooling system and irradiated for 3 h using a 300 W Xenon lamp under vigorous stirring. Electrons photogenerated by mg-$C_3N_4$ reduced Ag ions to elemental Ag nanoparticles, which were modified onto the holes and surface of the mg-$C_3N_4$ that were accessible to the SNA solution. The powder was subsequently filtered and repeatedly washed with deionized water. Ag/mg-$C_3N_4$ composite photocatalysts with different Ag mass ratios (1–5 wt%) were obtained after drying at 120 °C for 4 h under vacuum conditions. All reagents used in this study were analytical ones from licensed reagent companies.

### 2.2. Characterizations of the prepared mg-$C_3N_4$ and Ag/mg-$C_3N_4$ photocatalysts

The mesoporous structure of mg-$C_3N_4$ and the Ag modification information on mg-$C_3N_4$ was analyzed using a high-resolution transmission electron microscope (HRTEM, FEI Tecnai G20). The crystalline structures of the prepared mg-$C_3N_4$ and Ag/mg-$C_3N_4$ were identified through X-ray diffraction (XRD) (D/MAX-2500/PC; Rigaku Co., Tokyo, Japan). The elemental compositions of the 3 wt% Ag/mg-$C_3N_4$ were analyzed using a scanning electron microscope (SEM) (JSM-6700F; JEOL, Tokyo, Japan) with an energy dispersive spectrometer (EDS) (INCA Energy, OXFORD). The optical absorption properties of the photoelectrodes were investigated using a UV/vis diffuse reflectance spectrophotometer (U-41000; HITACHI, Tokyo, Japan). The photoluminescence intensity of the prepared samples was characterized using a fluorescence spectrometer (Fluoro Max-4, HORIBA Jobin Yvon).

### 2.3. Photocatalytic degradation of RhB

0.1 g prepared mg-$C_3N_4$ or Ag/mg-$C_3N_4$ was added to 100 mL RhB with a concentration of 10 mg $L^{-1}$ and stirred for 20 min.in the dark. The light source was a 300 W Xe arc lamp (PLS-SXE300, Beijing Changtuo Co. Ltd., Beijing, China). A flat circular quartz window with a diameter of 30 mm was on the side of the degradation reactor, and the photo passed through this window and illuminated on the RhB dye containing Ag/mg-$C_3N_4$ photocatalysts. A 420-nm cut-off filter was placed in front of the quartz window to remove light with wavelengths less than 420 nm and ultimately generate visible light. The distance between the light source and the dye liquid level is 8 cm. The temperature was maintained at 20 °C using circulating water. The absorbancy of RhB after centrifugation was measured every 5 min.

### 2.4. Photoelectrode preparation

An FTO glass (13 mm × 10 mm) was first ultrasonically cleaned with acetone of analytical grade for 5 min, rinsed with deionized water, and then dried with a clean, dry airflow. One longitudinal edge of the conductive side was then carefully covered with insulating tape, with the exposed effective area of the FTO glass measuring 1 $cm^2$. In total, 0.01 g of mg-$C_3N_4$ or Ag/mg-$C_3N_4$ powder was mixed with 0.1 mL of deionized water in an agate mortar, and the mixture was carefully ground for 10 min to form a homogeneous suspension. Then, 0.025 ml of the as-prepared suspension was evenly distributed onto the exposed area of the conductive side of the FTO glass. The insulating tape on the edge of the FTO glass was removed after the suspension had dried in the air. Finally, the FTO glass deposited with the as-prepared suspension was heated to 120 °C for 2 h under vacuum condition. A copper wire was connected to the conductive side of the FTO glass using conductive silver tape. Uncoated parts of the conductive side of the FTO glass were isolated with parafilm after the conductive silver tape had dried.

### 2.5. Electrochemical measurements

Electrochemical measurements were performed in a three-electrode experimental system using CHI660D Electrochemical Workstation (Shanghai Chenhua Instrument Co., Ltd., Shanghai, China). The prepared series photoelectrodes (1 cm × 1 cm), Ag/AgCl, and Pt electrode acted as the working, reference, and counter electrodes, respectively. The potentials are reported on the Ag/AgCl scale. The electrolyte was 0.5 mol $L^{-1}$ $Na_2SO_4$. The variations of the photoinduced current density with time (*i–t* curve) were measured at a 0 V bias potential under both white light (260 mW $cm^{-2}$) and visible light (200 mW $cm^{-2}$) illumination. The photo, generated by a 300 W Xe arc lamp (PLS-SXE300, Beijing Changtuo Co. Ltd., Beijing, China), passed through a flat circular quartz window, equipped on the side of the three-electrode cell, and illuminated on the backside of the photoelectrode. Visible light was obtained by placing a 420-nm cutoff filter in front of the quartz window to remove light with wavelengths less than 420 nm. Cyclic voltammetry (CV) curves of mg-$C_3N_4$ and 3 wt% Ag/mg-$C_3N_4$ were measured at the

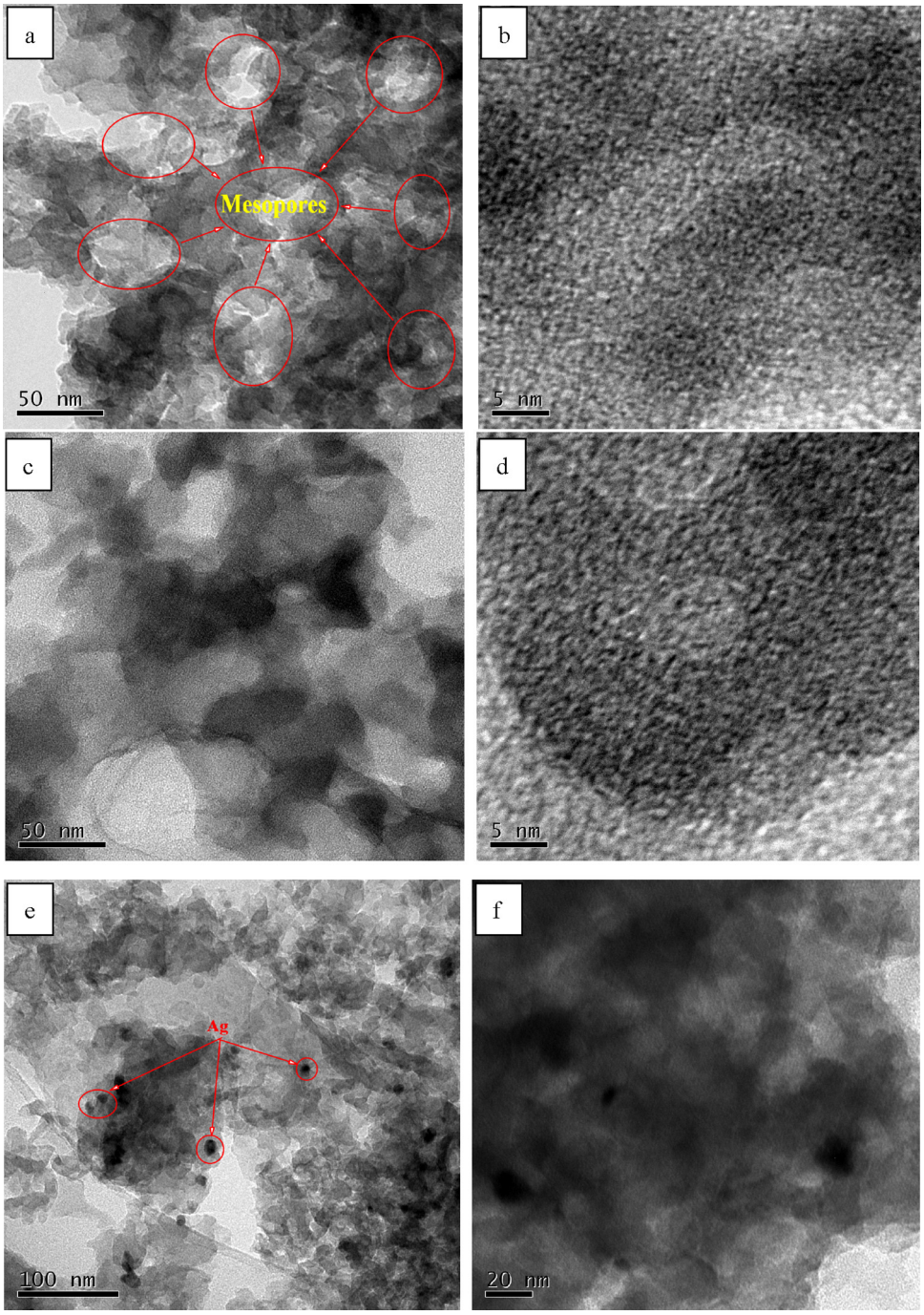


**Fig. 1.** HRTEM morphologies of mg-$C_3N_4$ (a and b), 3 wt% Ag/mg-$C_3N_4$ (c and d) and 5 wt% Ag/mg-$C_3N_4$ (e and f).

potential range of −1 to 1 V with the scanning rate of 50 mV $s^{-1}$. Electrochemical impedance spectroscopy (EIS) tests were performed at open circuit potential over the frequency range between $10^4$ and $10^{-1}$ Hz, with an AC voltage magnitude of 5 mV, using 12 points/decade. Mott–Schottky plots was measured at the potential range of −1.6 V to −0.2 V and the frequency of 10 Hz with an AC voltage magnitude of 10 mV.

## 3. Results and discussion

Fig. 1 shows HRTEM morphologies of the mg-$C_3N_4$ and Ag/mg-$C_3N_4$ photocatalysts. Fig. 1a shows the microscopic morphology of mg-$C_3N_4$ under low magnification. Many mesopores with a diameter of <50 nm were observed, which were formed by the etching of $SiO_2$ nanoparticles in this material. The HRTEM image of the mg-$C_3N_4$ under high magnification in Fig. 1b clearly shows mesoporous structures. Fig. 1c and d show the HRTEM morphologies of 3 wt% Ag/mg-$C_3N_4$ photocatalysts under both low and high magnification. The morphologies are similar to those of mg-$C_3N_4$ (Fig. 1a and b). Ag nanoparticles were not directly observed on the surface of the material, probably because of the formation of very small Ag particles. When the Ag modifying amount was increased to 5 wt%, approximately 10 nm Ag nanoparticles were observed on the mg-$C_3N_4$ surface (Fig. 1e and f). As mentioned in the experimental section, the SNA solution entered into the mesopores and micropores of mg-$C_3N_4$ and settled into these places. Ag ions would

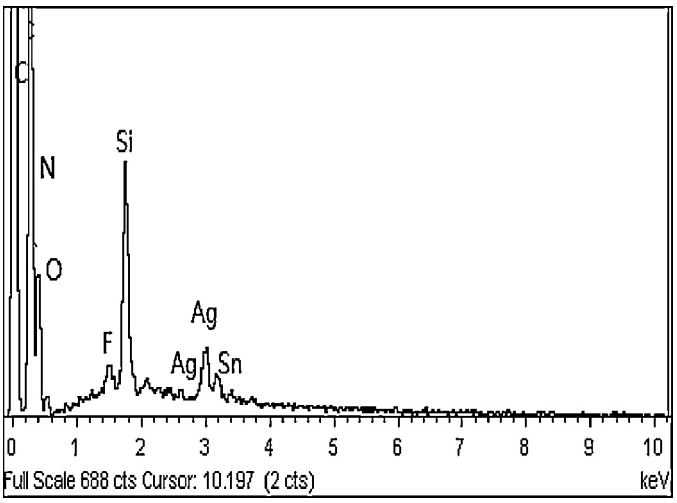


**Fig. 2.** EDS of the 3 wt% Ag/mg-$C_3N_4$ photoelectrode.

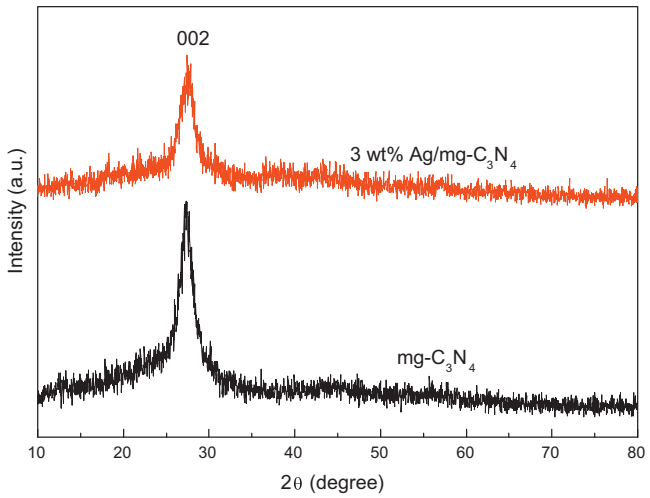


**Fig. 4.** XRD patterns of the mg-$C_3N_4$ and 3 wt% Ag/mg-$C_3N_4$.

be reduced by the photogenerated electrons of mg-$C_3N_4$ to elemental Ag in these tiny hole structures in the presence of visible light. Elemental Ag particles were deposited onto the walls of the holes and surface of mg-$C_3N_4$ that come into contact with the Ag-containing solution. When the Ag modifying amount was 3 wt%, the Ag ion concentration in the solution was low. Very small Ag particles were formed under this condition in the photoreduction process that ensued. When the Ag modifying amount was increased to 5 wt%, more free Ag ions came into contact with the mg-$C_3N_4$ surface. During the photo-assisted reduction process, a large amount of Ag molecules combined, and larger Ag particles formed on the mg-$C_3N_4$ surface, as observed by HRTEM (Fig. 1e and f).

Considering Ag nanoparticles were not observed on the surface of 3 wt% Ag/mg-$C_3N_4$, the existence of Ag was further proved using EDS and the CV curve of the photoelectrode prepared by depositing a 3 wt% Ag/mg-$C_3N_4$ photocatalyst onto the FTO conductive glass. Fig. 2 shows the EDS results of the photoelectrode prepared with a 3 wt% Ag/mg-$C_3N_4$ photocatalyst. Aside from carbon (C), nitrogen (N), tin, silicon, fluoride, and oxygen, which were produced by mg-$C_3N_4$, unetched $SiO_2$, and FTO conductive glass substrate, Ag elements were observed in the EDS results.

Fig. 3 shows the CV curves of the photoelectrodes prepared by mg-$C_3N_4$ and 3 wt% Ag/mg-$C_3N_4$ photocatalysts. No significant

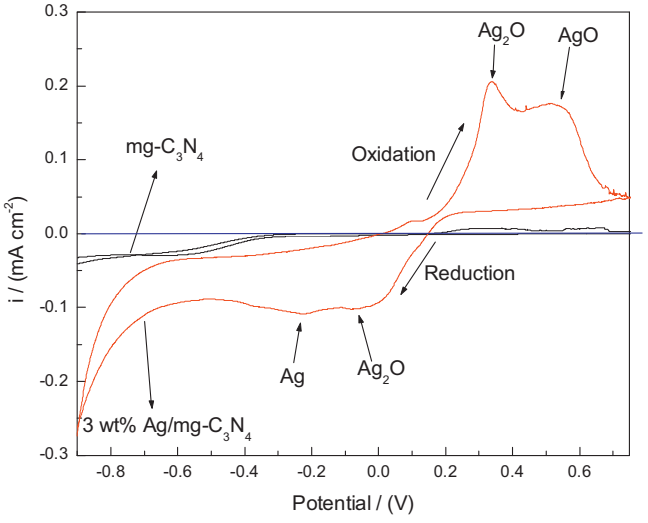


**Fig. 3.** Cyclic voltammograms of mg-$C_3N_4$ and 3 wt% Ag/mg-$C_3N_4$ in a 0.5 M $Na_2SO_4$ solution. Scan rate: 50 mV $s^{-1}$.

redox peaks were observed from the CV curve of mg-$C_3N_4$, which showed that mg-$C_3N_4$ has very high oxidation – reduction stability. After modifying 3 wt% Ag, a redox peak caused by the oxidation of Ag to $Ag_2O$ was observed at 0.34 V. With increased potential, another redox peak caused by the oxidation of $Ag_2O$ to AgO was observed at 0.53 V. A redox peak caused by the reduction of AgO to $Ag_2O$ was observed at −0.05 V. Another redox peak, caused by the reduction of $Ag_2O$ to Ag, was observed at −0.23 V. Therefore, based on the combined results of the EDS and CV curves, Ag was successfully modified on mg-$C_3N_4$ under such conditions. Ag could probably exist in both the holes of the mesoporous structure and the mg-$C_3N_4$ surface as super-small particles.

Fig. 4 shows the XRD patterns of the mg-$C_3N_4$ and 3 wt% Ag/mg-$C_3N_4$ photocatalysts. Strongest peak with $2\theta = 27.4^\circ$ was observed on both photocatalysts. This peak is the characteristic index of the interlayer stacking of aromatic series, indexed for graphitic materials as the 002 peak. Ag peaks were not observed for the 3 wt% Ag/mg-$C_3N_4$ photocatalysts. The highest processing temperature for Ag reduction in this work was 120 °C, which is much lower than the crystallization point of Ag. Xin et al. [38] reported that Ag peaks were observed in the X-ray diffraction (XRD) pattern only when the processing temperature was higher than 450 °C. At the same time, the Ag particles, prepared in this work, are too small and XRD pattern of Ag may be lost in background to recognize even it is crystalline. Thus, Ag peaks were not observed in the XRD pattern.

Fig. 5 shows the UV/vis diffuse reflectance spectra of mg-$C_3N_4$ and Ag/mg-$C_3N_4$ under various Ag-modifying amounts. Curve *a* shows the UV/vis diffuse reflectance spectrum of mg-$C_3N_4$. The maximum absorption wavelength can be got by drawing tangent along the critical fall part of the UV/vis diffuse reflectance spectrum and extending to the horizontal axis. According to curve *a*, the maximum absorption wavelength was approximately 475 nm, which indicates that mg-$C_3N_4$ responded to visible light. The maximum absorption wavelengths of the spectra of all Ag/mg-$C_3N_4$ (curves *b*–*d*) were approximately 475 nm, showing that Ag modification did not change the maximum absorption wavelength of mg-$C_3N_4$ and did not introduce new impurity energy levels to the valence band (VB) energy level. A plasmonic absorption peak normally caused by Ag nanoparticles and located at >450 nm was not observed in this study. In general, a significant plasmonic absorption peak could be observed only when the Ag nanoparticles were large enough and were modified into other materials with special morphological features [39,40]. The absence of this peak suggests that the modified Ag nanoparticles were ultrafine. Based on the vertical coordinates, the absorption value of Ag/mg-$C_3N_4$ appeared smaller than that

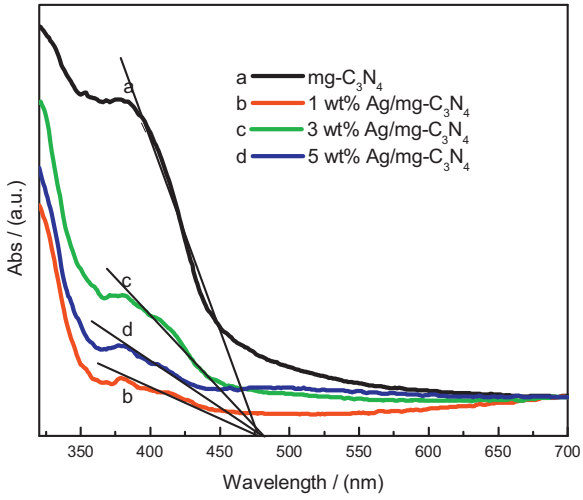


**Fig. 5.** UV/vis diffuse reflection spectra of the mg-$C_3N_4$ and Ag/mg-$C_3N_4$ with different Ag modifying amount.

of mg-$C_3N_4$. In fact, in the UV/vis diffuse reflectance tests for Ag/mg-$C_3N_4$, the horizontal lines after the end of the absorption were not in the zero position. All the spectra of Ag/mg-$C_3N_4$ were normalized to zero points and drew the curves together (Fig. 5).

Fig. 6 shows the RhB degradation curves of the photocatalysts of mg-$C_3N_4$ and Ag/mg-$C_3N_4$ with different Ag-modifying amounts (1–5 wt%) under visible light illumination ($\lambda > 420$ nm). Before the light was switched on, the photocatalysts were mixed with the RhB under dark conditions and stirred for 20 min. According to the data obtained for the 20 min.adsorption under dark conditions, the adsorption capacity of the Ag/mg-$C_3N_4$ catalysts was much higher than that of the mg-$C_3N_4$ catalysts. The 3 wt% Ag/mg-$C_3N_4$ photocatalyst showed the highest adsorption capacity. mg-$C_3N_4$ demonstrated an excellent capacity for the photocatalytic degradation of RhB. About 68% RhB was degraded by mg-$C_3N_4$ after 20 min.of illumination under visible light. Modifying mg-$C_3N_4$ with Ag significantly improved its photocatalytic degradation efficiency. As shown in Fig. 6, the photocatalytic degradation efficiency increased with increasing Ag-modifying amount and reached the maximum value when the Ag-modifying amount was 3 wt% (i.e., the optimal photocatalytic degradation efficiency). After only 20 min.of illumination by visible light, about 90% RhB was already degraded, and all of which was degraded after 25 min. Thus, modifying mg-$C_3N_4$ with just a small quantity of Ag significantly improved the adsorption capacity and photocatalytic degradation efficiency. With a further increase in Ag-modifying amount, both the adsorption capacity and photocatalytic degradation efficiency declined. As mentioned above, when the Ag-modifying amount was 3 wt%, very small Ag particles could exist in the holes and surface of mg-$C_3N_4$ to the extent that HRTEM cannot detect the existence of Ag in mg-$C_3N_4$. This Ag-modifying mode may be the reason for the significant promotion of the photocatalytic performance of mg-$C_3N_4$. When the Ag-modifying amount was increased to 5 wt%, numerous Ag molecules combined and formed Ag with larger particle sizes on the mg-$C_3N_4$ surface. This modifying mode decreased the effective contact region of Ag with mg-$C_3N_4$, the number of heterojunctions on the interface between Ag and mg-$C_3N_4$, and the active sites for photocatalytic reactions. Thus, the photocatalytic RhB degradation performance at this Ag-modifying amount was weaker than that at 3 wt%.

Ag modification significantly improved the visible-light photocatalytic RhB degradation performance of mg-$C_3N_4$ composite photocatalysts. The exceptionally high photocatalytic activity of Ag/mg-$C_3N_4$ photocatalysts shows potential for engineering applications. However, the promotion principle has not been fully explained. Thus, the effect of Ag on the photocatalytic processes and the improvements of the photoinduced electron–hole separation efficiency of Ag/mg-$C_3N_4$ should be further understood because of its profound significance in the applications and improvement of these photocatalyst materials.

The contribution of Ag modification to the effect of the photogenerated current densities of mg-$C_3N_4$ and Ag/mg-$C_3N_4$ thin-film photoelectrodes was studied under both white and visible light. Under the excitation of incident light, the processes of the photogenerated current of the thin-film photoelectrodes included the following steps: capturing photons, producing electron–hole pairs, separating and recombining electron–hole pairs, and transferring the separated electrons and holes in the thin film. These steps jointly determined the final value of the photogenerated current density.

In the following parts, 3 wt% Ag/mg-$C_3N_4$, which possesses the best degradation efficiency, was selected to further study the intrinsic mechanism for the role of Ag on the promotion of the photocatalytic and photoelectrochemical performance of mg-$C_3N_4$. mg-$C_3N_4$ was employed for a comparative investigation using photoelectrochemical and electrochemical test methods. Fig. 7 shows the photogenerated current densities of mg-$C_3N_4$

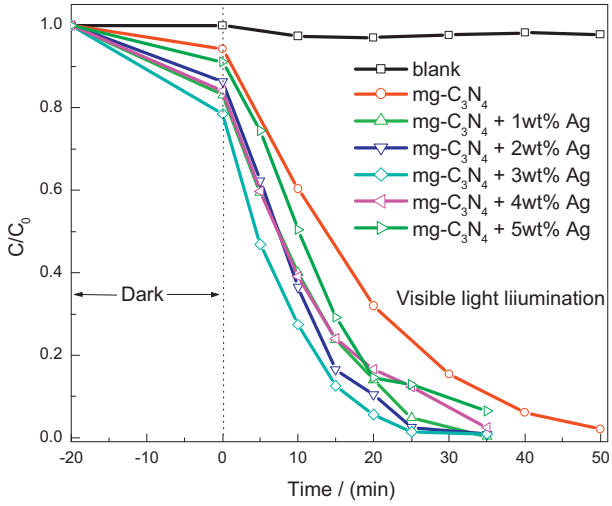


**Fig. 6.** Rhodamine B dye degradation curves of the mg-$C_3N_4$ and Ag/mg-$C_3N_4$ with different Ag modifying amount under visible light illumination.

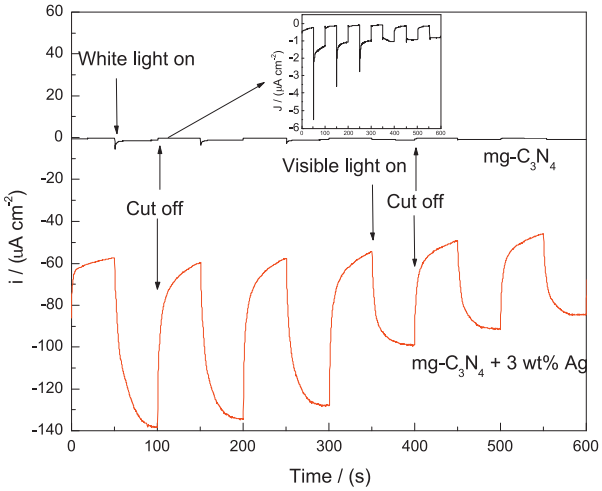


**Fig. 7.** Photogenerated current densities of the mg-$C_3N_4$ and 3 wt% Ag/mg-$C_3N_4$ thin-film photoelectrodes under white light and visible light on and off.

and 3 wt% Ag/mg-$C_3N_4$ thin-film photoelectrodes under white and visible light. The photogenerated current densities of mg-$C_3N_4$ under white and visible light were 2 and 1 μA cm$^{-2}$, respectively. Although mg-$C_3N_4$ exhibited an excellent capacity for the photocatalytic degradation of RhB, the photogenerated current densities of the mg-$C_3N_4$ thin-film photoelectrodes were very low. Thus, the mobility of the photogenerated electrons and holes in this polymeric material was very low, which enhanced their recombination. In the photocatalytic degradation of RhB, the photogenerated electrons and holes did not require long-distance migrations, as those in the thin-film photoelectrodes did. As long as the photogenerated electron–hole pairs were separated and transferred to the surface of the materials, the redox reactions with RhB around the materials occurred and achieved RhB degradation. The photogenerated current densities of the thin-film photoelectrodes prepared with the 3 wt% Ag/mg-$C_3N_4$ powder were 80 and 45 μA cm$^{-2}$ under white and visible light illumination, respectively, which were 40 and 45 times greater than those of mg-$C_3N_4$ thin-film photoelectrodes.

The photogenerated current densities of both mg-$C_3N_4$ and Ag/mg-$C_3N_4$ thin-film photoelectrodes exhibited a negative direction, indicating a cathodic current. This direction is the opposite direction of the current density generated by $TiO_2$ photoelectrodes. $TiO_2$ has a more positive VB potential. The photogenerated hole on $TiO_2$ after UV irradiation has a very strong oxidation capacity. Therefore, when the photogenerated holes are transferred to the surface of the material, they can be rapidly captured by the $OH^-$ ions ionized from water. Meanwhile, the photogenerated electrons migrate to the counter electrode, usually a Pt electrode, and react with the $H^+$ ions ionized from water to produce hydrogen. In contrast to $TiO_2$, mg-$C_3N_4$ has a more negative VB potential, which results in a relatively weaker oxidation capacity of its photogenerated holes. However, the photogenerated electrons, excited by light, possess very strong reduction ability and are thus quick to transfer to the surface of the materials and react with $H^+$ to produce hydrogen. Therefore, the mg-$C_3N_4$ photoelectrodes generated a cathodic current. Meanwhile, Ag has a relatively high work function. The photogenerated electrons of Ag/mg-$C_3N_4$ can be rapidly transferred to Ag, which can act as the catalytic center and accelerate the reduction of $H^+$ ions, thereby significantly increasing the photogenerated current density. The transfer of electrons to Ag improved the separation of the photogenerated electron–hole pairs, thereby improving the photocatalytic degradation performance.

EIS and the Mott–Schottky method were employed to determine how Ag modification improved the separation of the photogenerated electron–hole pairs. Furthermore, EIS can be used to study the migration ability of the electrons and the interface reaction ability of the electrons in the photocatalytic materials, which are very closely related to the photocatalytic and photoelectrochemical properties of semiconductor materials. Fig. 8 shows the EIS results for mg-$C_3N_4$ and 3 wt% Ag/mg-$C_3N_4$. Fig. 9 shows the equivalent circuit [41], which was established to fit the EIS results obtained in Fig. 8. In this equivalent circuit, $R_{sol}$ was the solution resistance; $R_t$ was the electron migration resistance in the thin-film photoelectrode; CPE was constant phase angle element. Its impedance was equal to $(Y_0(j\omega)^n)^{-1}$, where $\omega$ was the ac-voltage angular frequency (rad s$^{-1}$), and $Y_0$ and $n$ were the frequency-independent parameters. $R_{ss}$, $C_{ss}$ and $W_{ss}$ were used to describe the behaviors of the photogenerated electrons and holes on the interface between the semiconductor material and the electrolyte. $R_{ss}$, $C_{ss}$ and $W_{ss}$ were the electron transfer resistance on the interface, the interface capacitance and the Warburg resistance caused by the diffusion effect of the electrolyte, respectively. As showed in Fig. 8, the measured data are the dots with different symbols, while, the solid lines are the fitted results using the provided equivalent circuit. The measured data are fitted very well. Table 1 shows the

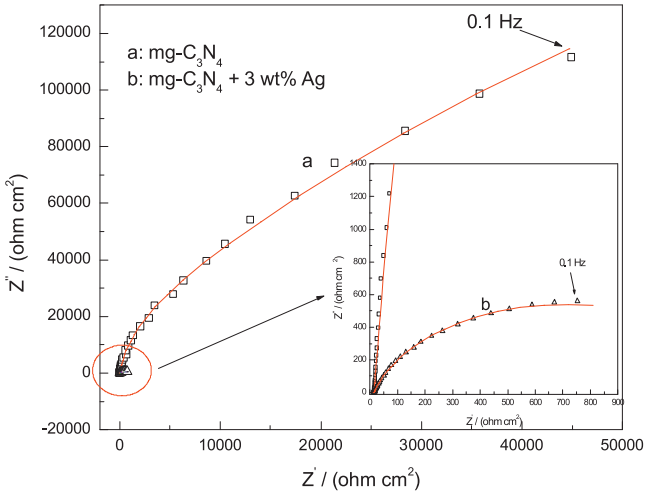


**Fig. 8.** EIS spectra of the mg-$C_3N_4$ and 3 wt% Ag/mg-$C_3N_4$.

parameters of the EIS data. The $R_t$ value obtained for mg-$C_3N_4$ was $3.311 \times 10^5$ Ω cm$^2$ (Table 1). After modifying with 3 wt% Ag, the $R_t$ value decreased to $3.810 \times 10^3$ Ω cm$^2$, which is two orders of magnitude lesser than the material without Ag. The decrease of the $R_t$ value indicated that Ag modification significantly increased the conductivity of mg-$C_3N_4$. In the mg-$C_3N_4$ polymer, C and N are connected to each other by both single and double bonds, similar to the bonding structure of the conductive polymer polyaniline. The conductivity of eigenstate polyaniline is very low. However, doping polyaniline with some impurity elements or introducing proton acids into polyaniline chains resulted in an increase of several orders of magnitude in its conductivity [42]. In the present study, Ag modification induced adsorption at the position of the N components of mg-$C_3N_4$, which changed the density of the electron cloud distribution of the molecular chain [43] and increased the conductivity of mg-$C_3N_4$ to some extent. Furthermore, the $C_{ss}$ value changed significantly because of Ag modification. Before Ag modification, the $C_{ss}$ value was $1.071 \times 10^{-6}$ μF cm$^{-2}$. After modifying with 3 wt% Ag, the $C_{ss}$ value increased to $5.267 \times 10^2$ μF cm$^{-2}$, which is an increase of approximately eight orders of magnitude. The increase in the interfacial capacitance indicated that the density of the surface state significantly increased after Ag modification. The surface state significantly influences the photoelectrochemical reactions and can capture photogenerated electrons or holes, thereby increasing the separation efficiency of the photogenerated electron–hole pairs. Furthermore, the surface state could act as the catalytic center and accelerate surface reactions. In this paper, Ag exhibited a very low hydrogen production resistance. When the photogenerated electrons of mg-$C_3N_4$ were transferred to Ag, the electrons rapidly reduced water to produce hydrogen under the catalysis of Ag, resulting in rapid interface reactions. The interfacial electron transfer resistance ($R_{ss}$) value decreased to 6.204 Ω cm$^2$ after Ag modification, that is, the interfacial reactions had almost

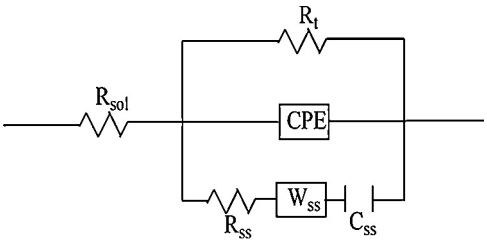


**Fig. 9.** The equivalent circuit for fitting the EIS results of the mg-$C_3N_4$ and 3 wt% Ag/mg-$C_3N_4$ photoelectrodes in $NaSO_4$ electrolyte.

**Table 1**
Fitted parameters of the EIS of mg-$C_3N_4$ and 3 wt% Ag/mg-$C_3N_4$ photoelectrodes in 0.5 M $Na_2SO_4$ solution.

| Sample | $R_{sol}$ ($\Omega$ cm$^2$) | $R_t$ ($\Omega$ cm$^2$) | $Q$ ($\Omega^{-1}$ cm$^{-2}$ s$^n$) | $n$ | $C_{ss}$ ($\mu$F cm$^{-2}$) | $R_{ss}$ ($\Omega$ cm$^2$) | $W_{ss}$ ($\Omega$ cm$^2$) |
|---|---|---|---|---|---|---|---|
| mg-$C_3N_4$ | 15.17 | $3.311 \times 10^5$ | $1.059 \times 10^{-5}$ | 0.9636 | $1.071 \times 10^{-6}$ | $7.372 \times 10^{11}$ | 0.06474 |
| mg-$C_3N_4$ + Ag | 9.004 | $3.810 \times 10^3$ | $7.786 \times 10^{-4}$ | 0.3479 | $5.267 \times 10^2$ | 6.204 | 0.01137 |

no resistance (Table 1). However, before Ag modification, the $R_{ss}$ of mg-$C_3N_4$ reached $7.372 \times 10^{11}$ $\Omega$ cm$^2$, indicating that the interface reaction energy was too high. Thus, the photogenerated current density was very low.

Ag modifying on the mg-$C_3N_4$ material surface caused strong surface states. Considering the Fermi levels of these surface states differed from that of mg-$C_3N_4$, Ag modifying on the mg-$C_3N_4$ surface established a new interfacial electric field and caused changes in the mg-$C_3N_4$ level potential. In this paper, Mott–Schottky method was employed to study relation between capacitance of the space charge region and the applied potential. The description of the specific formula is as follows:

$$\frac{1}{C^2} = 2(e\varepsilon\varepsilon_0 N_D)^{-1} \cdot \left(E - E_{fb} - \frac{\kappa T}{e}\right) \quad (1)$$

where $C$ is the capacitance of the space charge region in the semiconductor; $N_D$ is the electron carrier density, e is the elemental charge, $\varepsilon_0$ is the permittivity of free space, $\varepsilon$ is the relative permittivity of the semiconductor, $E$ is the applied potential, $E_{fb}$ is the flat band potential, $T$ is the temperature, and $\kappa$ is the Boltzmann constant.

The flatband potential of a semiconductor material can be determined by extrapolating to $C^{-2} = 0$. The flatband potentials of mg-$C_3N_4$ and 3 wt% Ag/mg-$C_3N_4$ were approximately $-1.33$ and $-1.02$ V, respectively (Fig. 10). Thus, Ag modifying on the mg-$C_3N_4$ surface positively shifted the flatband potential.

According to the tangent slopes in Fig. 10, both mg-$C_3N_4$ and 3 wt% Ag/mg-$C_3N_4$ photoelectrodes exhibited the characteristics of n-type semiconductors, which agreed with those from Zhang et al. [44]. However, as showed in Fig. 7, both mg-$C_3N_4$ and 3 wt% Ag/mg-$C_3N_4$ photoelectrodes generated negative current under illumination, which showed the characteristics of p-type semiconductor. It is well known that the Fermi level of a semiconductor will change with the applied bias potential. If an n-type semiconductor modified on a conductive substrate, the semiconductor would gather positive charges and the conductive substrate would gather negative charges when the applied bias potential increased from negative direction. At this time, the Fermi level of this

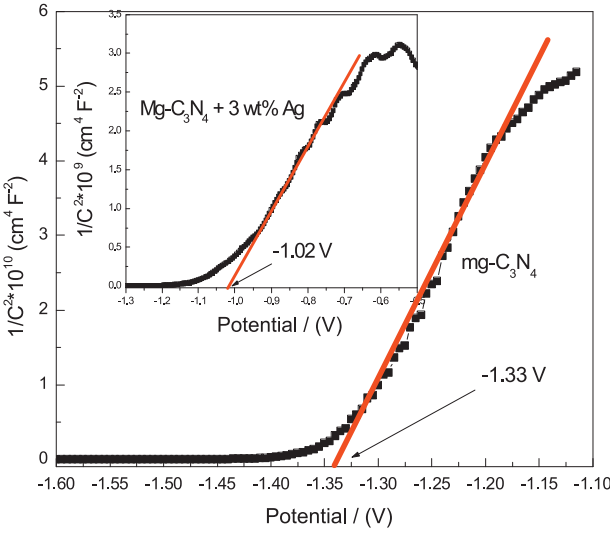


**Fig. 10.** Mott–Schottky plots of the mg-$C_3N_4$ and 3 wt% Ag/mg-$C_3N_4$ photoelectrodes.

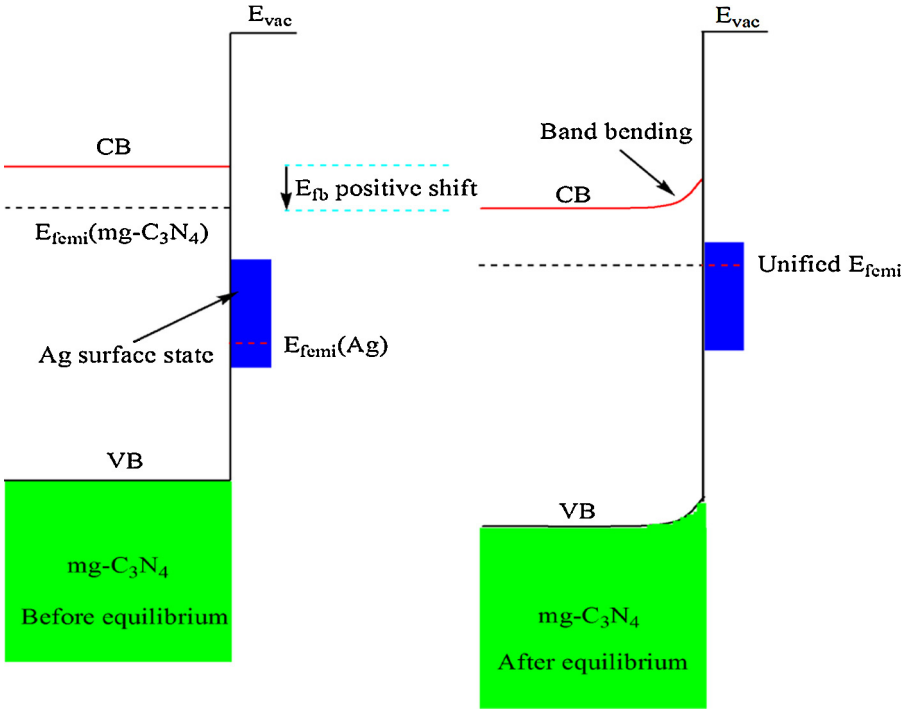


**Fig. 11.** Schematic illustration of the positive shift of the electron energy level when the Ag modified on mg-$C_3N_4$.

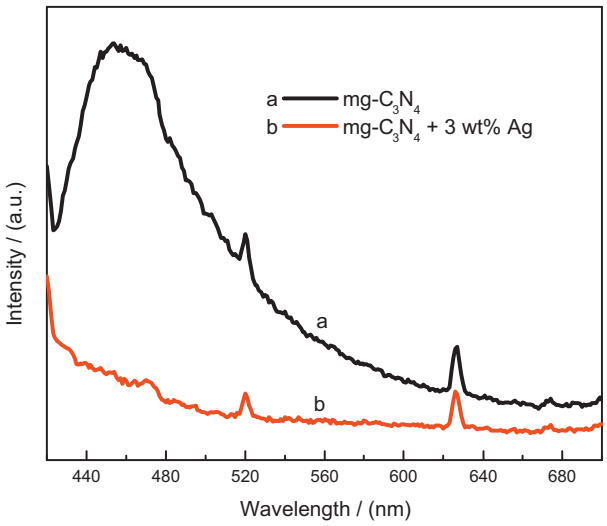


**Fig. 12.** Photoluminescence spectra of mg-$C_3N_4$ and 3 wt% Ag/mg-$C_3N_4$.

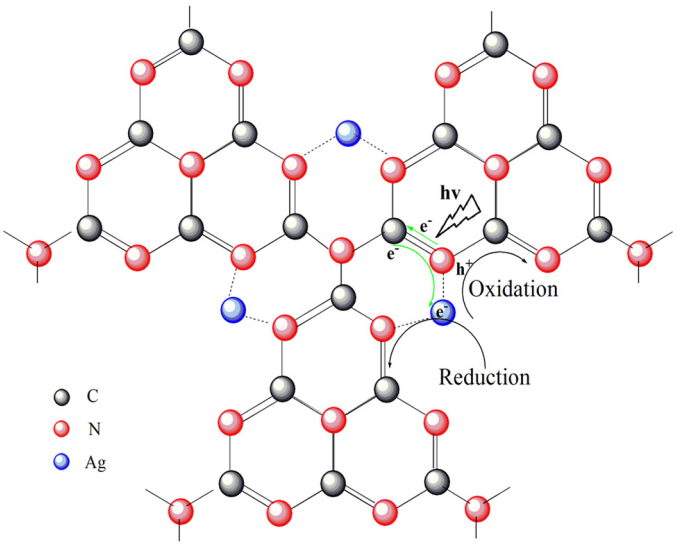


**Fig. 13.** Proposed mechanism for the promotion of the photocatalytic RhB degradation performance of mg-$C_3N_4$ by Ag modification.

semiconductor will positively shift and move close to the valence band of the semiconductor, and the semiconductor type was converted from n type into p type. In Fig. 7, the bias potential was 0 V (versus Ag/AgCl). The Fermi levels of mg-$C_3N_4$ and 3 wt% Ag/mg-$C_3N_4$ were positive shifted and the characteristics of them exhibited as a p type.

Fig. 11 shows a schematic of the positive shift of the electron energy level with Ag modifying on mg-$C_3N_4$. mg-$C_3N_4$ exhibited the characteristics of an n-type semiconductor, as well as a very negative conduction band (CB) potential. The Fermi level of mg-$C_3N_4$ is located under the CB. Because the Fermi level of Ag is more positive than the CB potential of mg-$C_3N_4$, the Fermi levels of Ag and mg-$C_3N_4$ shifted forward when Ag was modified on the mg-$C_3N_4$ surface [43]. When the Fermi level of mg-$C_3N_4$ shifted to the positive direction, it pulled the CB in the same direction. The surface electrons of mg-$C_3N_4$ transferred to Ag from the interface between Ag and mg-$C_3N_4$ and enriched Ag. The CB formed an upward band bending close to the interface between mg-$C_3N_4$ and Ag. When the electron exchange was in equilibrium, $E_{fb}$ positively shifted (Fig. 11). Considering electrons were transferred at the interface between mg-$C_3N_4$ and Ag, the interfacial electric field must be formed there. The existence of this interfacial electric field would significantly enhance the efficiency of the photogenerated electron–hole separation and prolong the lifetime of the photoinduced electrons.

Fig. 12 shows the photoluminescence spectroscopy of mg-$C_3N_4$ and 3 wt% Ag/mg-$C_3N_4$. For mg-$C_3N_4$, a strong, luminous broad peak emerged at 440–500 nm, and two weaker peaks at 520 and 626 nm, respectively. For 3 wt% Ag/mg-$C_3N_4$, the light-emitting broad peak at 440–500 nm was absent. The luminous intensities of the peaks at 520 and 626 nm were significantly weakened. Thus, the presence of Ag can effectively inhibit the annihilation of the photogenerated electron–hole pairs and effectively improve their separation efficiency and the lifetime of the photogenerated electrons, thereby enhancing the RhB photocatalytic degradation efficiency and photoelectrochemical properties of Ag/mg-$C_3N_4$.

Fig. 13 schematically shows the proposed mechanism for the promotion of the photocatalytic RhB degradation performance of mg-$C_3N_4$ by Ag modification. The outer layer of the N component of mg-$C_3N_4$ has a lone electron pair. The 5 S sublayer in the outermost layer of the electronic structure of Ag is an empty band that easily accepts lone electron pairs from the N components to form a stable N–Ag key structure. This bond can enhance the conductivity of mg-$C_3N_4$ on the one hand and can accelerate the electron transfer between mg-$C_3N_4$ and Ag on the other. The Fermi level of Ag differs from that of mg-$C_3N_4$, and Ag modifying on mg-$C_3N_4$ will shift the Fermi levels. The energy band of mg-$C_3N_4$ will bend, and an effective interfacial electric field will form, which can effectively enhance the photogenerated electron–hole separation efficiency and lifetime of the photogenerated electrons. Considering Ag can lower down the energy barriers of reduction reactions, it can be used as the catalytic center for such reactions when the photogenerated electrons are transferred to Ag. The possible reaction mechanisms are listed in the following: [33]

$$Ag \rightarrow Ag^+ + e^- \quad (2)$$

$$e^- + O_2 \rightarrow {}^\bullet O_2^- \quad (3)$$

$$\text{mg-}C_3N_4 + hv \rightarrow e_{cb}^- + h_{vb}^+ \quad (4)$$

$$Ag^+ + e_{cb}^- \rightarrow Ag \quad (5)$$

$$h_{vb}^+ + OH^- \rightarrow {}^\bullet OH \quad (6)$$

Ag was first oxidized to $Ag^+$ by dissolved oxygen, which obtained electrons and was converted to $^\bullet O^{2-}$. Subsequently, $^\bullet O^{2-}$ participated in further dye reduction reactions. The photogenerated electrons, $e_{cb}^-$, were excited to the CB of mg-$C_3N_4$, and the photogenerated holes, $h_{vb}^+$, remained in the VB of mg-$C_3N_4$. Subsequently, the $e_{cb}^-$ were transferred to the oxidized $Ag^+$, and $Ag^+$ was reduced to Ag again. $h_{vb}^+$ was captured by the $OH^-$ ionized from water, which produced $^\bullet OH$ free radicals with very strong oxidation capacities. $^\bullet OH$ free radicals affect the oxidation degradation of dyes. After these steps, the reduction reaction processes of the photocatalytic reactions were accelerated by Ag modification, thereby improving the photocatalytic and photoelectrochemical performance of mg-$C_3N_4$.

Electrochemical measurements were performed in a three-electrode experimental system using CHI660D Electrochemical Workstation (Shanghai Chenhua Instrument Co., Ltd., Shanghai, China). The prepared series photoelectrodes (1 cm × 1 cm), Ag/AgCl, and Pt electrode acted as the working, reference, and counter electrodes, respectively. The potentials are reported on the Ag/AgCl scale. The electrolyte was 0.5 mol $L^{-1}$ $Na_2SO_4$. The variations of the photoinduced current density with time ($i$–$t$ curve) were measured at a 0 V bias potential under both white light (260 mW $cm^{-2}$) and visible light (200 mW $cm^{-2}$) illumination. The photo, generated by

a 300 W Xe arc lamp (PLS-SXE300, Beijing Changtuo Co. Ltd., Beijing, China), passed through a flat circular quartz window, equipped on the side of the three-electrode cell, and illuminated on the backside of the photoelectrode. Visible light was obtained by placing a 420-nm cutoff filter in front of the quartz window to remove light with wavelengths less than 420 nm. Cyclic voltammetry (CV) curves of mg-$C_3N_4$ and 3 wt% Ag/mg-$C_3N_4$ were measured at the potential range of −1 to 1 V with the scanning rate of 50 mV $s^{-1}$. Electrochemical impedance spectroscopy (EIS) tests were performed at open circuit potential over the frequency range between $10^4$ and $10^{-1}$ Hz, with an AC voltage magnitude of 5 mV, using 12 points/decade. Mott–Schottky plots was measured at the potential range of −1.6 to −0.2 V and the frequency of 10 Hz with an AC voltage magnitude of 10 mV.

## 4. Conclusions

Ag nanoparticles were successfully modified on mg-$C_3N_4$ by photo-assisted reduction. The photoelectric conversion performance of mg-$C_3N_4$ and Ag/mg-$C_3N_4$ were studied using the *i–t* curve, EIS, CV, Mott–Schottky plot, HRTEM, SEM/EDS, XRD, UV/vis diffuse reflectance spectroscopy and photoluminescence spectroscopy.

The main conclusions can be drawn in the following:

(1) Ag-modifying on mg-$C_3N_4$ significantly increased its photoelectric conversion performance. The best performance of Ag/mg-$C_3N_4$ was obtained when the Ag modifying amount is 3 wt%. Under visible light, the photogenerated current density of 3 wt% Ag/mg-$C_3N_4$ is approximately 45 times greater than that of mg-$C_3N_4$.
(2) The 3 wt% Ag/mg-$C_3N_4$ possessed the best photocatalytic RhB degradation efficiency. Only after 20 min, about 90% RhB have been degraded and all RhBs had been degraded after 25 min under visible light.
(3) Modifying Ag on mg-$C_3N_4$ increased the migration rate of the photogenerated electrons and interfacial electron transfer ability. A heterojunction electric field was formed on the interface between modified Ag and mg-$C_3N_4$, enhanced the separation efficiency of the photogenerated electron-hole pairs and prolonged the lifetime of the photogenerated electrons, which eventually made a significant promotion of its photoelectric conversion performance.
(4) In the aspect of Ag improving the photoelectric conversion performance, Ag nanoparticles in smaller size are much more effective than those in larger size.

## Acknowledgements

This work was financially supported by the Hundreds-Talent Program of the Chinese Academy of Sciences (Y02616101L).

## References

[1] M.R. Hoffmann, S.T. Martin, W. Choi, D.W. Bahnemann, Chemical Reviews 95 (1995) 69.
[2] H. Gerischer, Electrochimica Acta 38 (1993) 3.
[3] Z. Liu, X. Zhang, S. Nishimoto, T. Murakami, A. Fujishima, Environmental Science and Technology 42 (2008) 8547.
[4] Z. Zhang, Yuan, G. Shi, Y. Fang, L. Liang, H. Ding, L. Jin, Environmental Science and Technology 41 (2007) 6259.
[5] Y. Wang, X. Li, G. Lu, X. Quan, G. Chen, Journal of Physical Chemistry C 112 (2008) 7332.
[6] T.F. Jaramillo, S.H. Baeck, A. Kleiman-Shwarsctein, W.E. McFarland, Macromolecular Rapid Communications 25 (2004) 297.
[7] I.S. Cho, Z. Chen, A.J. Forman, D.R. Kim, P.M. Rao, T.F. Jaramillo, X. Zheng, Nano Letters 11 (2011) 4978.
[8] J.H. Park, S. Kim, A.J. Bard, Nano Letters 6 (2006) 24.
[9] H.M. Chen, C.K. Chen, Y.C. Chang, C.W. Tsai, R.S. Liu, S.F. Hu, W.S. Chang, K.H. Chen, Angewandte Chemie International Edition 49 (2010) 5966.
[10] X. Yang, A. Wolcott, G. Wang, A. Sobo, R.C. Fitzmorris, F. Qian, J.Z. Zhang, Y. Li, Nano Letters 9 (2009) 2331.
[11] A. Wolcott, W.A. Smith, T.R. Kuykendall, Y. Zhao, J.Z. Zhang, Advanced Functional Materials 19 (2009) 1849.
[12] E.S. Kwak, W. Lee, N. Park, J. Kim, H. Lee, Advanced Functional Materials 19 (2009) 1093.
[13] Y.J. Kim, M.H.G. Lee, Lim Y.S. Choi, N.G. Park, K. Kim, W.I. Lee, Advanced Materials 21 (2009) 3668.
[14] M. Law, L.E. Greene, J.C. Johnson, R. Saykally, P. Yang, Nature Materials 4 (2005) 455.
[15] G. Liu, Y. Zhao, C. Sun, F. Li, G.Q. Lu, H.M. Cheng, Angewandte Chemie International Edition 47 (2008) 4516.
[16] J. Choi, H. Park, M.R. Hoffmann, Journal of Physical Chemistry C 114 (2010) 783.
[17] K.G. Kanade, B.B. Kale, J.O. Baeg, S.M. Lee, C.W. Lee, S.J. Moon, H. Chang, Materials Chemistry and Physics 102 (2007) 98.
[18] W.T. Sun, Y. Yu, H.Y. Pan, X.F. Gao, Q. Chen, L.M. Peng, Journal of the American Chemical Society 130 (2008) 1124.
[19] M. Seol, H. Kim, W. Kim, K. Yong, Electrochemistry Communications 12 (2010) 1416.
[20] W. Wang, X. Huang, S. Wu, Y. Zhou, L. Wang, H. Shi, Y. Liang, B. Zou, Applied Catalysis B: Environmental 134–135 (2013) 293.
[21] G. Li, D. Zhang, J.C. Yu, Chemistry of Materials 20 (2008) 3983.
[22] L. Ge, C., Han, J. Liu, App. Catal. B: Envireon. 108-109 (2011) 100.
[23] L. Zhang, K.H. Wang, Z. Chen, J.C. Yu, J. Zhao, C. Hu, C.Y. Chan, P.K. Wong, Applied Catalysis A: General 363 (2009) 221.
[24] Y. Hou, X. Li, Q. Zhao, X. Quan, G. Chen, Advanced Functional Materials 20 (2010) 2165.
[25] H. Lv, L. Ma, P. Zeng, D. Ke, T. Peng, Journal of Materials Chemistry 20 (2010) 3665.
[26] X.C. Wang, K. Maeda, A. Thomas, K. Takanabe, G. Xin, J.M. Carlsson, K. Domen, M. Antonietti, Nature Materials 8 (2009) 76.
[27] X. Wang, X. Chen, A. Thomas, X. Fu, M. Antonietti, Advanced Materials 21 (2009) 1609.
[28] Y. Zhang, T. Mori, L. Niu, J. Ye, Energy & Environmental Science 4 (2011) 4517.
[29] Y.Z. Zhang, T. Mori, J.H. Ye, M. Antonietti, Journal of the American Chemical Society 132 (2010) 6294.
[30] F. Goettmann, A. Fischer, M. Antonietti, A. Thomas, Angewandte Chemie International Edition 45 (2006) 4467.
[31] X. Wang, K. Maeda, X. Chen, K. Takanabe, K. Domen, Y. Hou, X. Fu, M. Antonietti, Journal of the American Chemical Society 131 (2009) 1680.
[32] H. Yan, J. Yang, G. Ma, G. Wu, X. Zong, Z. Lei, J. Shi, C. Li, Journal of Catalysis 266 (2009) 165.
[33] Y. Zheng, L. Zheng, Y. Zhan, X. Lin, Q. Zheng, K. Wei, Inorganic Chemistry 46 (2007) 6980.
[34] Y. Di, X. Wang, A. Thomas, M. Antonietti, ChemCatChem 2 (2010) 834.
[35] M. Yoshida, A. Yamakata, K. Takanabe, J. Kubota, M. Osawa, K. Domen, Journal of the American Chemical Society 131 (2009) 13218.
[36] J. Dong, M. Wang, X. Li, L. Chen, Y. He, L. Sun, ChemSusChem 5 (2012) 2133.
[37] L. Ge, C. Han, J. Liu, Y. Li, Applied Catalysis A: General 215 (2011) 409–410.
[38] B. Xin, L. Jing, Z. Ren, B. Wang, H. Fu, Journal of Physical Chemistry B 109 (2005) 2805.
[39] K. Awazu, M. Fujimaki, C. Rockstuhl, J. Tominaga, H. Murakami, Y. Ohki, N. Yoshida, T. Watanabe, Journal of the American Chemical Society 130 (2008) 1676.
[40] H.A. Atwater, A. Polman, Nature Materials 9 (2010) 205.
[41] V. Spagnol, E. Sutter, C. Debiemme-Chouvy, H. Cachet, B. Baroux, Electrochimica Acta 54 (2009) 1228.
[42] J.F. Huang, H. Luo, C. Liang, I.W. Sun, G.A. Baker, S. Dai, Journal of the American Chemical Society 127 (2005) 12784.
[43] Z. Zhang, J.T. Yates, Chemical Reviews 112 (2012) 5520, Volume: [43].
[44] J. Zhang, X. Chen, K. Takanabe, K. Maeda, K. Domen, J.D. Epping, X. Fu, M. Antonietti, X. Wang, Angewandte Chemie International Edition 49 (2010) 441.